

Femtosecond response time measurements of a Cs_2Te photocathode

A. Aryshev,* M. Shevelev, Y. Honda, N. Terunuma, and J. Urakawa
KEK: High Energy Accelerator Research Organization, 1-1 Oho, Tsukuba, Ibaraki 305-0801, Japan

We present the response time measurements of a Cs_2Te photocathode illuminated with two ~ 100 fs duration, variable time separation laser pulses at 266 nm wavelength. The response time was confirmed in dispersive region downstream of a 12-cell standing wave S-band acceleration structure using a well-known RF zero-crossing technique. At the same time it was also measured by changing mechanical path-length difference between two micro-bunches. Both methods agree that Cs_2Te photocathode time response is of the order of 250 fs and thereby it is possible to generate and control a THz sequence of relativistic electron bunches by a conventional S-band RF gun. This result further opens a possibility to construct wide-range tunable THz FEL.

PACS numbers: 41.75.Ht, 07.57.Hm, 42.72.Ai

Keywords: RF gun; Semiconductor photocathode

In the present time the importance of further development of the new high brightness compact relativistic electron sources is rapidly growing. The main optimization factors along with charge and brightness are operational lifetime of the photocathodes as well as short temporal response and low transverse intrinsic emittance of generated electron beam [1, 2]. The improvements of the photocathode RF gun technology have made a significant impact for X-ray FELs [3], novel light sources and future colliders design [4, 5]. Also it has become crucial technology for table-top accelerator-based X-ray and Coherent radiation sources for medical [6] and biological [7] use. The generation of a high-brightness THz-frequency coherent radiation pulses (when the radiation intensity is proportional to the number of particles per bunch squared [8]) is strongly connected to generation of a short electron bunches. Usually to obtain such conditions different bunch compression methods are used [9, 10]. However this requires significant beamline space allocation and notably increases overall facility cost. That is why consideration of another approach to generate short electron bunches directly illuminating a photocathode with femtosecond duration laser pulses become attractive. Also it is possible to consider a pre-bunched or co-called comb electron beam generation on a single RF accelerating field cycle what requires photocathode irradiation with a THz sequence of a several tens fs-length electron bunches. The application of such a beam is very wide since it can be used to generate an intense spectrum-tunable THz pulses and even give enhancement to radiation emission [11, 12]. Space-charge dominated electron beam properties is expected throughout initial acceleration in RF gun [13] and also the minimum bunch duration will be determined by the photocathode response time and laser pulse duration. Further acceleration of the comb beam by a radio-frequency (RF) accelerating field with gradient of the order of 50 MV/m when carried on a single RF accelerating field cycle enables to accelerate particles to 5 MeV in a 7.5 cm RF gun. Another important feature of the pre-bunched beam should

be continuously variable time separation between micro bunches, square envelope of the and amplitude modulation possibility within the micro-pulse sequence. What sets significant limits on the laser pulse stacking method. Previously reported schemes are based on usage of a compact birefringent crystal arrays [14, 15] and interferometric schemes. In the reality, crystal-based approach when the input pulse is decomposed in two orthogonally polarized pulses with a time separation proportional to the crystal length does not make continuous time separation control possible due to limited number of crystal's length. While interferometer-based schemes are usually more mechanically advanced and requires tighter alignment, they can provide necessary pulse control [16, 17].

Photocathode properties are usually dictating RF gun laser system output pulse energy, wavelength (harmonic), polarization and pulse duration what adds additional limitations for the laser system. Over the last decade many photocathode materials were tested. Nowadays the main choice of material revolves around a few options: metals (Cu , Mg), positive electron affinity (PEA) semiconductors, like Cs_2Te and Cs_3Sb and negative electron affinity (NEA) semiconductors, like $GaAs$ [18]. Typically metals have long life-time, short time-response, high damage threshold, but low quantum efficiency (Q.E.). NEA photocathodes are operated in visible spectrum, have high Q.E., but sensitive for oxidation hence require ultra-high vacuum operation and have a long response time. PEA photocathodes, especially Cs_2Te also have a good resistance to laser damage and have lower dark current than most of the other semiconductor photocathodes. As it is usually reported [19] they have a comparatively shorter response time of the order of picoseconds whereas there is no principle limitations for it not to be rather fast [20].

In this letter, we demonstrate for the first time that, the response time of the relatively high Q.E. Cs_2Te photocathode is faster than ~ 250 fs, and thereby it is possible to generate and control a THz sequence of a few hundred femtoseconds relativistic electron bunches by a

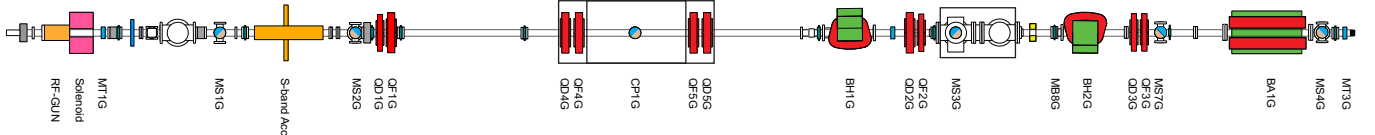


FIG. 1. LUCX beamline.

conventional S-band RF gun. The result further widens the potential of designing a truly table-top THz FEL based on super-radiant undulator [11] or Smith-Purcell radiation [21].

The measurements presented in this paper was done at the Laser Undulator Compact X-ray facility (LUCX) at High Energy Accelerator Research Organization (KEK). LUCX schematic diagram is shown in Fig. 1. It is a multipurpose linear electron accelerator facility initially constructed as a RF gun test bench and later extended to facilitate Compton scattering [22] and coherent radiation generation [23] experiments. It consists of a high mode separation 3.6 cell RF gun [24], which was designed to produce a multi-bunch high quality electron beam with up to 1000 bunches, a 0.5 nC bunch charge, and 10 MeV beam energy. This beam can be then accelerated to 30 MeV by the normal conductivity 1 m 12-cell mode-separated linac booster [25]. Two klystrons (Toshiba E 3729 and Toshiba E3712) are used to independently feed RF gun and accelerating structure. Also, two laser systems: picosecond Nd:YAG and femtosecond Titanium-Sapphire were employed to make possible different LUCX operation modes. Table I summarizes electron beam parameters usually obtained in femtosecond operation mode of the LUCX.

TABLE I. LUCX parameters in fs operation mode

Beam energy, typ.	8 MeV
Intensity / 4 micro-bunches	100 pC
Number of micro-bunches, max	16
Bunch length, max	1 ps
Bunch length, min	50 fs
Normalized emittance, $\epsilon_x \times \epsilon_y$	$4.7 \times 6.5 \pi \text{mm mrad}$

The cathode preparation system is well described in [26]. This system of a commonly used type to supply Cs_2Te cathodes for RF guns manufactured at many institutes worldwide. Molybdenum was used as the substrate for the best cathode resulting parameters [27]. The cathode was initially mechanically polished with fine diamond powder during manufacturing. Before $Cs - Te$ evaporation it was cleaned by Ar^+ bombardment in the ultra-high-vacuum. During the fabrication process, the substrate was held at 25C. The evaporation process includes a ~ 10 nm film of Te deposition on the substrate surface with subsequent activation by Cs until Q.E. reaches a few percent level. However due to Cs quick diffusion and oxi-

dation resulting Q.E. was stabilized at a 0.3% level. This number was confirmed by both xenon lamp and electron beam measurements.

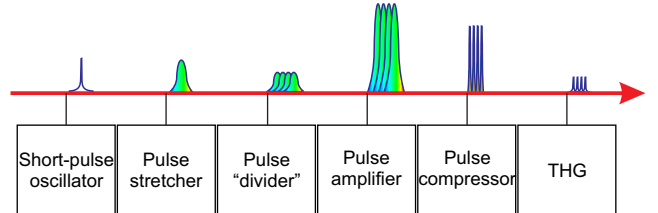


FIG. 2. CPA technique with micro-pulse extension.

To generate a sequence of femtosecond micro-bunches the well-established Titanium-Sapphire "Chirped Pulse Amplification" technique [28] laser system was chosen, Fig.2. Short pulses of a few tens femtoseconds from the oscillator are temporarily stretched to a picosecond level before they are amplified in RGA up to a few μJ . We have introduced "pulse divider" (PD) right after the RGA so pulses are splitted and recombined with controllable delay by the double-pass Michelson interferometer, Fig.3 (left), where linear polarizations are denoted as s and p , and s/p represents a mixed polarization states. This minor modification allows generating sequence of a spectrally chirped picosecond pulses with variable time separation. After that they are amplified up to 2 mJ per micro-pulse by the multi-pass Ti:Sa amplifier and recompressed back to a few tens femtoseconds. This is possible due to the same micro-pulses polarizations after multi-pass amplifier. As a result 1.3 mJ of each micro-pulse energy at Ti:Sa fundamental harmonic (FH) was available at the laser system output. Also the laser system was extended to allow direct measurement of a generated micro-pulse durations and its time separations by the method based on the registration of the Second Harmonic energy cross distribution produced in nonlinear crystal [32]. Resulting cross-correlations give calibrated [33] absolute temporal measurements which is then compared with electron beam measurements. In case of micro-pulsed input the cross-correlation dependence has an additional peaks symmetric around the main correlation. The time separation between main correlation and the satellite peak is equal to the real time separation between micro-pulses. The TH diagnostics includes laser spot imaging (Fig.3, right) at the distance equivalent to the cathode (co-called "virtual cathode") and pulse en-

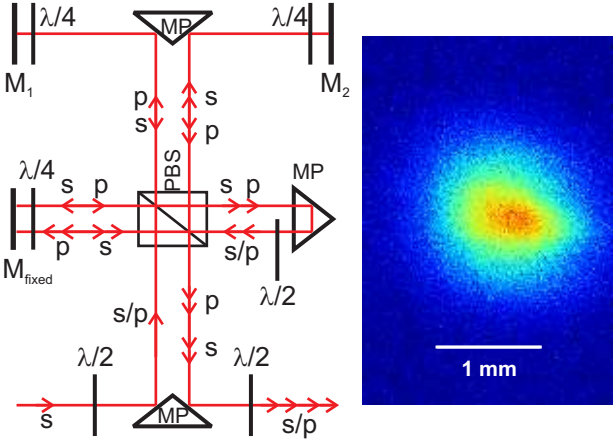


FIG. 3. Pulse divider general scheme (left) and typical $500 \times 500 \mu\text{m}$ rms UV profile at virtual cathode (right). Abbreviations: *PBS* - polarized beam splitter, *MP* - prism mirror, M_1 and M_2 motorized mirrors, M_{fixed} fixed mirror, $\lambda/2$ and $\lambda/4$ half-wave and quarter-wave retardation plates respectively.

ergy measurements.

In the current configuration PD can produce four micro pulses with time separation proportional to the pass difference of the interferometer arms. To avoid confusion in experimental results interpretation half of the interferometer fixed arm and both motorized arms were blocked to produce a single laser pulse for energy calibration, Fig.4. For the rest of the data only half of the interferometer fixed arm was blocked to output two micro-pulses. In this case only one movable mirror M_2 determines time separation between pulses and the relative time offset is proportional to two times the movable mirror displacement. The 25 nm spectral bandwidth of each picosecond laser pulses when separated by more than 70 fs ensures no longitudinal interference between micro-pulses [29] what in turn gives uniform pulse intensities within the micro-train unlike presented in [30].

To confirm electron beam parameters the quasi-ballistic electron optics was designed. This optics makes 5 mm horizontal dispersion at the *MS3G* 300 μm -thick *YAG* screen which is located beyond *BH1G* bending magnet after the linac booster. Initially linac booster was switched off and the transverse electron density distribution as a dependence of *BH1G* dipole magnet current was measured, Fig.4. This shows initial electron beam center-of-mass energy is equal to $E = 8.25 \pm 0.002$ MeV and energy spread is $dE = 18.8 \pm 0.2$ keV, i.e. $dE/E \sim 0.2\%$.

The rms electron bunch length is measured by the zero-phasing technique [34], in which a time correlated energy chirp is applied on the bunch by modulated quasi-linear RF electric field. The bunch is then dispersed by a dipole

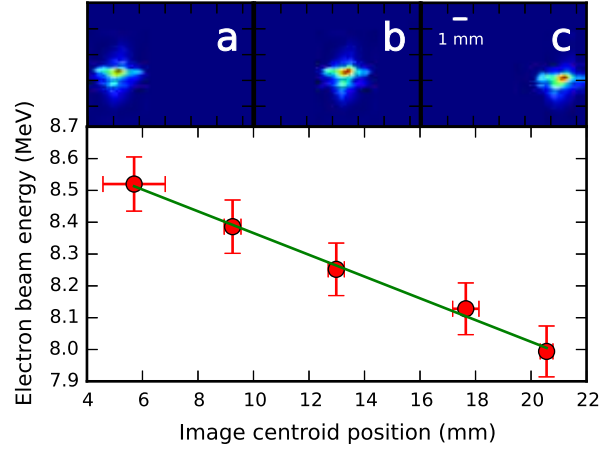


FIG. 4. Top row: transverse electron density distribution measured for (a) 6.96 A, (b) 6.76 A, (c) 6.56 A *BH1G* dipole magnet current. Bottom: Image centroid position versus *BH1* dipole magnet field strength (recalculated to the electron beam energy) with linear fit: amplitude 8.71 ± 0.02 and slope $-3.41 \cdot 10^{-2} \pm 1.48 \cdot 10^{-3}$.

magnet *BH1G* so that the different time slices of the electron bunch are projected onto a scintillating *YAG* screen at different horizontal positions, and thus beam image on the screen shows the intensity distribution of the electron bunch along its temporal direction. To confirm RF zero-crossing point a few *MS3G* images for RF power-off and RF power-on were taken. Comparison of Fig.5 (a) and (d) shows that the energy deviation is small in this case. To estimate bunch length the correlation of the RF phase with image centroid shift on *MS3G* screen was measured. Typical beam images are shown on Fig.5 (c), (d), (e). The linear approximation of this correlation effectively gives scale of the horizontal image size in RF degrees, what in turn can be recalculated to the time scale as follows. The linear slope of the calibration is 6.036 ± 0.32 mm/deg. what is 6.206 ± 0.33 $\mu\text{m}/\text{fs}$ or 0.161 ± 0.008 $\text{fs}/\mu\text{m}$ assuming 1deg. S-band (2856 MHz) RF is 972.6 fs.

However these measurements are affected by initial energy distribution within the bunch. Large energy spread will lead to compressed-like image around RF 0 deg. phase and decompressed-like image around RF 180 deg. phase. To cross-check given calibration additional mechanical calibration method was developed. The method is based on one micro-bunch arrival time change and recording bunch-to-bunch distance change on *MS3G* while the linac booster RF phase is set to 0 deg. The sequence of *MS3G* images shows gradual movement of the "movable arm bunch" from left to right, i.e. from low to high energy (while the "fixed arm bunch" remains its position), Fig.6 top row. Simultaneously the FH laser pulses cross-correlations were acquired to confirm micro-

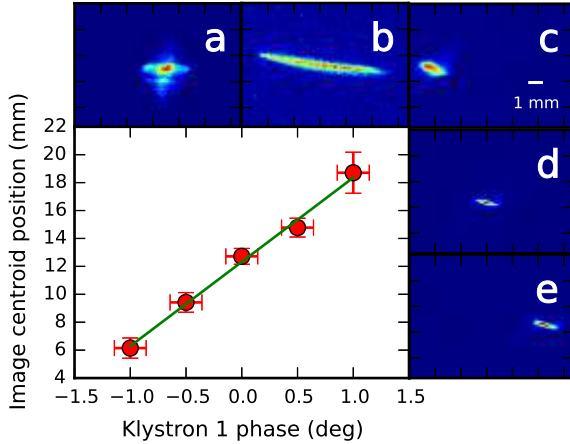


FIG. 5. Electron density distribution measured for (a) RF power off, (b) 180 deg. RF crossing, (c) -1 deg. accelerating phase, (d) 0 deg. accelerating phase, (e) +1 deg. accelerating phase. Bottom left: Beam image centroid position plotted as a function of RF phase with linear fit: slope 6.036 ± 0.32 mm/deg.

pulse spacings, Fig.6, bottom inset. As can be seen, this technique gives very close scale factor of $0.156 \pm 5.43 \cdot 10^{-3}$ fs/um for *MS3G* horizontal image size.

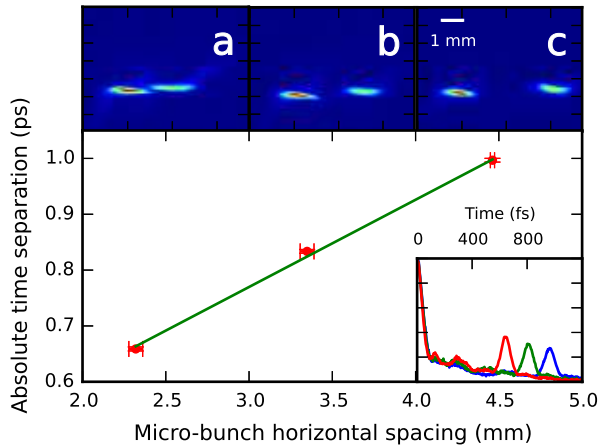


FIG. 6. Two micro-bunch electron density distribution measured for (a) 4.7 mm, (b) 4.725 mm, (c) 4.750 mm *M1* mirror positions. Bottom: Micro-bunch horizontal spacing versus micro-bunch time separation with linear fit: slope $0.156 \pm 5.43 \cdot 10^{-3}$ fs/um. Inset: two laser micro-pulse cross-correlation taken for the same *M1* mirror positions.

Following notation given in [34], Eq.7, the real longitudinal rms bunch length can be expressed through the ratio of initial phase-space slope and the RF slope $|C1|/|C0| = X_{rms}^+ - X_{rms}^- / X_{rms}^+ + X_{rms}^-$ as:

$$\sigma_z = \frac{X_{rms}^+ + X_{rms}^-}{2|C_0|} = \frac{X_{rms}^+ - X_{rms}^-}{2|C_1|}, \quad (1)$$

where $X_{rms}^+ = 3637.89 \pm 119.34$ μm and $X_{rms}^- = 592.04 \pm 4.77$ μm are rms image sizes measured for 180 deg. and 0 deg. RF phases as shown on Fig.5 (b) and (d) respectively. Assuming that the phase-space slope $C1 = 1$, the real electron bunch length is 1522.93 ± 119.43 μm and hence the *Cs₂Te* photocathode response time estimate is 245.19 ± 22.66 fs by RF zero-crossing calibration and 237.57 ± 20.12 fs by the mechanical calibration. At the same time it is possible to write another simple evaluation of the real bunch length bearing in mind that compression and decompression rates C_{rate} are equal at 0 deg. and 180 deg. RF phases as:

$$\sigma_z = X_{rms}^- \cdot C_{rate} = \frac{X_{rms}^+}{C_{rate}} \text{ or } \sigma_z = \sqrt{X_{rms}^+ \cdot X_{rms}^-} \quad (2)$$

From this, the real electron bunch length is 1467.57 ± 119.43 μm and hence the *Cs₂Te* photocathode response time estimate is 236.28 ± 22.52 fs by RF zero-crossing and 228.94 ± 20.01 fs by the mechanical calibrations. What is consistent with above results within standard deviations. All errors are statistical errors which are not accounting for any systematic effects.

In conclusion, our measurements shows that the response time of the *Cs₂Te* photocathode is of the order of ~ 250 fs as have been confirmed by two independent calibration methods. The result further widens the potential of designing a table-top tunable THz FEL based on super-radiant coherent radiation. With no doubts space-charge effects play a fundamental role in preservation of the temporal structure of the comb electron beam and limits the maximum achievable beam charge. The further work on higher charge per bunch is desired for strong THz radiation generation. It can be done by increasing of the RF gun acceleration gradient and optimization of the laser spot size at the photocathode.

The authors would like to thank A. Araki and M. Fukuda for their valuable help, useful discussions and support of the LUCX accelerator operation and maintenance. This work was supported by Photon and Quantum Basic Research Coordinated Development Program from the Ministry of Education, Culture, Sports, Science and Technology, Japan and JSPS KAKENHI grant numbers 23226020 and 24654076.

* Corresponding author: alar@post.kek.jp

- [1] I.V. Bazarov, B.M. Dunham, C.K. Sinclair, Phys. Rev. Lett. 102, 104801 (2009).
- [2] D.H. Dowell, I. Bazarov, B. Dunham, K. Harkay, C. Hernandez-Garcia, R. Legg, H. Padmore, T. Rao,

J.Smedley, W.Wan, Nucl. Instrum. Methods Phys. Res., Sect. A 622, 685 (2010).

[3] C. Hauri, New developments for FEL photo injector, seeding, THz laser systems, proc. FEL11, Shanghai, (2011).

[4] N. Phinney, N. Toge, N. Walker, International Linear Collider Reference Design Report Volume 3, Tech. Rep. (2007).

[5] P. Tenenbaum and T. Shintake, Annual Review Nuclear Particle Physics 49, 125 (1999).

[6] P. H. Siegel, IEEE Trans. Microw. Theory Tech., 52, 2438 (2004).

[7] S. W. Smye, J.M. Chamberlain, A.J. Fitzgerald, E. Berry, Phys. Med. Biol. 46, R101-R112 (2001).

[8] G. L. Carr, M. C. Martin, W. R. McKinney, K. Jordan, G. R. Neil and G. P. Williams, Nature 420, 153-156 (2002).

[9] Y. Ding, A. Brachmann, F.J. Decker, D. Dowell, P. Emma, J. Frisch, S. Gilevich, G. Hays, Ph. Hering, Z. Huang, et al., Phys. Rev. Lett. 102, 254801 (2009).

[10] E. Chiadroni, M. Bellaveglia, P. Calvani, M. Castellano, L. Catani, A. Cianchi, G. Di Pirro, M. Ferrario, G. Gatti, O. Limaj, et al., Rev. Sci. Instrum., 84, 022703 (2013).

[11] M. Arbel, A. Abramovich, A. L. Eichenbaum, A. Gover, H. Kleinman, Y. Pinhasi, I. M. Yakover, Phys. Rev. Lett. 86, 2561 (2001).

[12] D. Li, M. Hangyo, Y. Tsunawaki, Z. Yang, Y. Wei, S. Miyamoto, M.R. Asakawa, K. Imasaki, Nucl. Instrum. Methods Phys. Res., Sect. A 674, 20 (2012).

[13] L. Serafini , Nucl. Instr. and Meth. in Phys. Res. A 340, 40 (1994).

[14] B. Dromey, M. Zepf, M. Landreman, K. O'Keeffe, T. Robinson, and S. M. Hooker, Applied Optics 46, 5142 (2007).

[15] A. K. Sharma, T. Tsang, and T. Rao, Phys. Rev. ST Accel. Beams 12, 033501 (2009).

[16] C. W. Siders, J.L. Siders, A.J. Taylor, S.G. Park, and A.M. Weiner, Applied Optics 37, 5302 (1998).

[17] S. Liu, Y.C. Huang, Nucl. Instr. and Meth. in Phys. Res. A 637, S172-S176 (2011).

[18] R.A. Loch, Cesium-Telluride and Magnesium for high quality photocathodes, Master Thesis, University of Twente (2005).

[19] S.H. Kong, J. Kinross-Wright, D.C. Nguyen, R.L. Sheffield, Nucl. Instrum. Methods Phys. Res., Sect. A 358, 272 (1995).

[20] J. E. Clendenin, T. Kotseroglou, G.A. Mulholland, D.T. Palmer, J.F. Schmerge, SLAC-PUB-8355.

[21] S. E. Korbly, A. S. Kesar, J. R. Sirigiri, R. J. Temkin, Phys. Rev. Lett. 94, 054803 (2005).

[22] K. Sakaue, M. Washio, S. Araki, M. Fukuda, Y. Higashi, Y. Honda, T. Omori, T. Taniguchi, N. Terunuma, J. Urakawa and N. Sasao, Rev. Sci. Instrum. 80, 123304, (2009).

[23] A. Aryshev, S. Araki, M. Fukuda, P. Karataev, A. Konkov, G. Naumenko, A. Potylitsyn, K. Sakaue, L. Sukhikh, N. Terunuma, et al., Nucl. Instr. and Methods in Phys. Res. section A, 763, 424 (2014).

[24] A. Deshpande, S. Araki, M. Fukuda, K. Sakaue, N. Terunuma, J. Urakawa, and M. Washio, Phys. Rev. ST Accel. Beams, 14, 063501 (2011).

[25] M. Fukuda, S. Araki, A. Deshpande, Y. Higashi, Y. Honda, K. Sakaue, N. Sasao, T. Taniguchi, N. Terunuma, J. Urakawa, Nucl. Instr. and Methods in Phys. Res. section A, 637, S67 (2011).

[26] N. Terunuma, A. Murata, M. Fukuda, K. Hirano, Y. Kamiya, T. Kii, M. Kuriki, R. Kuroda, H. Ohgaki, K. Sakaue, et al., Nucl. Instrum. Methods Phys. Res., Sect. A 613, 1 (2010).

[27] E. Chevallay, J. Durand, S. Hutchins, G. Suberlucq, H. Trautner, KEK APAC TH4046 972 (1998).

[28] S. Backus, C.G. Durfee, M.M. Murnane and H.C. Kapteyn, Rev. Sci. Instrum., 69, 1207 (1998).

[29] M. Born and E. Wolf, Principles of optics, 4th. ed, Pergamon Press, London, (1970).

[30] Y. Shen, X. Yang, G.L. Carr, Y. Hidaka, J. B. Murphy, X. Wang, Phys. Rev. Lett. 107, 204801 (2011).

[31] W. Seka, S.D. Jacobs, J.E. Rizzo, R. Boni, R.S. Craxton, Optics Communications 34, 3, 469 (1980).

[32] C. Kolmeder, W. Zinth, W. Kaiser, Optics Communications, 30, 3, 453 (1979).

[33] F. Salin, P. Georges, G. Roger, and A. Brun, Applied Optics 26, 4528 (1987).

[34] D. X. Wang, G.A. Krafft, C.K. Sinclair, Phys. Rev. E 57, 2283 (1998).